OH-Stretch Vibrational Spectroscopy of Hydroxymethyl Hydroperoxide

Juliane L. Fry,[†] Jamie Matthews,[‡] Joseph R. Lane,[§] Coleen M. Roehl,[||] Amitabha Sinha,*[,‡] Henrik G. Kjaergaard,*[,§] and Paul O. Wennberg*[,||,⊥]

Arthur Amos Laboratory of Chemical Physics, California Institute of Technology, Pasadena, California 91125, Department of Chemistry and Biochemistry, University of California—San Diego, 9500 Gilman Drive, La Jolla, California 92093-0314, Department of Chemistry, University of Otago, P.O. Box 56, Dunedin, New Zealand, Division of Geological and Planetary Sciences, California Institute of Technology, Pasadena, California 91125, and Division of Engineering and Applied Science, California Institute of Technology, Pasadena, California 91125

Received: February 25, 2006; In Final Form: April 12, 2006

We report measurement and analysis of the photodissociation spectrum of hydroxymethyl hydroperoxide ($HOCH_2OOH$) and its partially deuterated analogue, $HOCD_2OOH$, in the OH-stretching region. Spectra are obtained by Fourier transform infrared spectroscopy in the $1\nu_{OH}$ and $2\nu_{OH}$ regions, and by laser induced fluorescence detection of the OH fragment produced from dissociation of $HOCH_2OOH$ initiated by excitation of the $4\nu_{OH}$ and $5\nu_{OH}$ overtone regions (action spectroscopy). A one-dimensional local-mode model of each OH chromophore is used with ab initio calculated OH-stretching potential energy and dipole moment curves at the coupled-cluster level of theory. Major features in the observed absorption and photodissociation spectra are explained by our local-mode model. In the $4\nu_{OH}$ region, explanation of the photodissocation spectrum requires a nonuniform quantum yield, which is estimated by assuming statistical energy distribution in the excited state. Based on the estimated dissociation threshold, overtone photodissociation is not expected to significantly influence the atmospheric lifetime of hydroxymethyl hydroperoxide.

Introduction

Hydroperoxides are important trace constituents of the urban and global atmosphere. They play important roles in oxidation chemistry as both reservoirs and sinks of OH radical and odd oxygen.[1−3] Organic peroxides are also oxidants in their own right, oxidizing SO_2 in clouds, fogs, or rain,[4,5] and are believed to have a toxic effects on plants.[2]

In the gas phase, H_2O_2 and the organic hydroperoxides are formed via recombination reactions of peroxy radicals (HO_2, RO_2). In the troposphere, peroxy radicals are produced primarily by photooxidation of CO and volatile organic compounds by the hydroxyl radicals.[6] Because the peroxy radicals are removed via reactions with NO and NO_2, the production rate of hydroperoxides via this mechanism tends to be lower in polluted atmospheres.[6]

Recent investigations have found that, in the presence of water, the ozonolysis of isoprene and other alkenes can also produce hydroperoxides.[7−12] Although these alkene ozonolysis reactions remain poorly understood, it is thought that they involve the formation of a carbonyl oxide (or Criegee biradical) which subsequently reacts with water to form peroxide. Observations of H_2O_2 and other organic hydroperoxides after sunset, when model calculations showed ozonolysis to be the dominant source of peroxides, provide evidence for this mechanism.[13] The smallest stabilized Criegee biradical, CH_2OO, formed in the ozonolysis of ethene and terminal alkenes, is believed to react with water to form hydroxymethyl hydroperoxide ($HOCH_2OOH$ or HMHP):

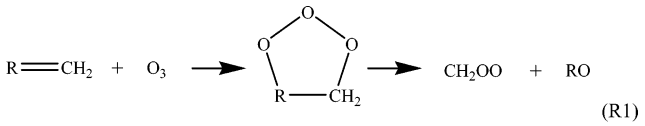

(R1)

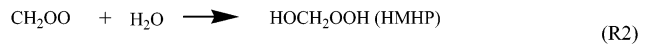

(R2)

Hydroxymethyl hydroperoxide has been identified in the atmosphere but its atmospheric abundance is quite uncertain.[13−27] HMHP concentrations as high as 5 ppbv were measured in the southeastern United States when high concentrations of ozone and isoprene were present.[18] More recent studies have reported smaller concentrations, for example, a median HMHP value of 1 ppbv during the 1995 Southern Oxidants Study campaign in Nashville, TN,[16] maximum HMHP mixing ratio of 0.2 ppbv during the 1998 BERLIOZ campaign in Pabstthum, Germany,[13] and HMHP undetected during ESCOMPTE (2001) and BOND (2002) campaigns in Marseilles, France.[14] Some of these results may be spurious, however, as measurement of HMHP and other organic peroxides is challenging and sampling artifacts have been reported.[1]

The atmospheric fate of HMHP and its role in the transport of continental boundary-layer pollutants to more remote environments is determined by the relative rates of the various HMHP loss processes. Photolysis (and to a lesser extent reaction with OH[28]) tends to recycle the radical pool, while wet and dry

* To whom correspondence should be addressed: E-mail: asinha@ucsd.edu, henrik@alkali.otago.ac.nz, and wennberg@gps.caltech.edu.
[†] Arthur Amos Laboratory of Chemical Physics, California Institute of Technology.
[‡] University of California—San Diego.
[§] University of Otago.
[||] Division of Geological and Planetary Sciences, California Institute of Technology.
[⊥] Division of Engineering and Applied Science, California Institute of Technology.

10.1021/jp0612127 CCC: $33.50
Published on Web 05/17/2006

deposition are permanent sinks of HO_x. Direct measurements of HMHP removal by reaction with OH are very difficult since HMHP is unstable. An estimated 298 K lifetime for reaction with OH of about 2 days is derived from the comparable rate coefficient for reaction of OH with CH_3OOH.[28] Efficient removal of HMHP by wet and dry deposition is expected because of its high solubility.[29] Photolysis rates for HMHP in the UV were first estimated by Su et al.,[30] who observed $HOCH_2OOH$, during experiments on the photooxidation of formaldehyde. Absorption cross-sections of HMHP vapor were later reported between 205 and 360 nm.[28] Photolysis of HMHP is expected to yield OH and $HOCH_2O$ radical products, which react further with atmospheric O_2:

$$HOCH_2OOH + h\nu \rightarrow HOCH_2O + OH \qquad (R3)$$

$$HOCH_2O + O_2 \rightarrow HCOOH + HO_2 \qquad (R4)$$

Thus, photolysis of $HOCH_2OOH$ results in release of two molecules of HO_x from the reservoir peroxide.

In this study, we evaluate the importance of vibrational overtone photodissociation of HMHP as a sink of HMHP and a source of HO_x. We make use of a frequency tunable photolysis laser system that is coupled to sensitive measurements of OH radical products using laser-induced fluorescence (LIF). This technique has been used previously to evaluate the magnitude of the atmospheric HO_x source from overtone photolysis of HO_2-NO_2 and other gases.[31−35] We study the vibrational overtone initiated decomposition of HMHP excited in the third ($4\nu_{OH}$) and fourth ($5\nu_{OH}$) overtone regions of the OH-stretching vibrations. We supplement this study with Fourier transform infrared absorption spectroscopy of the $1\nu_{OH}$ and $2\nu_{OH}$ regions.

To facilitate assignment of the spectra, we have calculated the OH-stretching transitions using an anharmonic oscillator local-mode model with parameters and dipole moment functions obtained from ab initio coupled cluster calculations. The local-mode model has been successful in the description and analysis of XH-stretching (where X = C, N, O) overtone spectra.[36−38] With the use of experimental local-mode parameters and dipole moment functions calculated at modest ab initio levels, relative intensities within a given overtone were obtained.[39] More recently, empirically scaled ab initio calculated local-mode parameters combined with ab initio dipole moment function have been successful in predicting OH-stretching spectra of hydrated complexes.[40,41] The advancement in computational methods and hardware now allows high-level ab initio calculations, which can eliminate the need for empirical scaling of the local-mode parameters. For example, the OH-stretching local-mode parameters of the different conformers in ethylene glycol were recently calculated with impressive agreement to experiment.[42]

Experiment

The method for synthesis of HMHP (and the partially deuterated analogue, HMHP-d_2) is based on that originally described by Bauerle and Moortgat.[28] A low flow of N_2 is passed over 5 g of paraformaldehyde powder (Aldrich) (or the deuterated analogue, paraformaldehyde-d_2, Aldrich) at 100 °C and subsequently bubbled for ∼15 h through a glass vessel containing 7 mL of 90−95% H_2O_2 in H_2O at 60 °C. Excess H_2O_2 was maintained during the synthesis to avoid formation of bis-HMHP ($HOCH_2OOCH_2OH$).[43] The synthesis was monitored by FTIR to ensure minimal bis-HMHP formation. The resulting liquid sample is immediately placed in a glass U-tube for the experiments. To prevent injury in case of a peroxide explosion, the sample U-tube is housed in a Plexiglass box. The sample is pumped at the highest possible pumping speed for several hours prior to photolysis experiments to remove remaining H_2O, HCOOH, and H_2O_2 contamination and then flowed into the photolysis chamber, which is maintained at typical pressures of 60−80 mTorr for experiments. A bulb of water behind a valve is connected to the top of the U-tube above the sample and outside of the sample box. After each experiment is finished, the peroxide residue is quenched with water prior to any handling. **Extreme caution should be exercised when working with concentrated samples of peroxides. The water quenching method is highly recommended; this was implemented after an explosion occurred when a concentrated HMHP sample was vented to atmospheric pressure.**

In the flow system, HMHP undergoes unimolecular dissociation on the ground electronic surface after absorbing a near-IR or visible photon, and the resulting OH fragment is probed via LIF.[44] Laser light for excitation of the third or fourth OH overtone region, $4\nu_{OH}$ or $5\nu_{OH}$, is generated by a dye laser (Continuum ND60) pumped by the second harmonic of a Nd:YAG laser (Continuum NY82-20), operating in the region of 600−650 nm (Rhodamine 640 + DCM mixture, 40 mJ/pulse) and 720−770 nm (LDS750 + LDS765 mixture, 20 mJ/pulse, bandwidth of ∼0.08 cm^{-1}). The OH photofragments are probed via the A−X transition at ∼308 nm using LIF. The 0.13 cm^{-1} bandwidth probe radiation is provided by frequency doubling the output of a second Nd:YAG (Continuum NY81-20) pumped dye laser (Continuum ND60). The pump−probe delay is fixed at 80 ns (20 ns) for the $4\nu_{OH}$ ($5\nu_{OH}$) spectroscopy experiments reported here. The OH fluorescence is collected using an *f*/1 lens system imaged onto an end-on photomultiplier tube (EMI 9813QB). The signal from the PMT is sent to a gated charge integrator (LeCroy, 2249SG analog-to-digital converter) and digitized for computer data collection. These $4\nu_{OH}$ and $5\nu_{OH}$ spectroscopy measurements were conducted at the University of California, San Diego.

Near and mid-IR absorption spectra are obtained in a 2-meter path length absorption cell using a Nicolet (Magna-IR 560) FTIR spectrometer. A small droplet of the HMHP sample is added to the cell and, after the majority of the HCOOH, H_2O, and H_2O_2 impurity is pumped off, spectra are obtained in the range 1000−11000 cm^{-1} using either an extended KBr or a CaF_2 beam splitter and an MCT-A detector. These $1\nu_{OH}$ and $2\nu_{OH}$ spectroscopy measurements were conducted at the California Institute of Technology.

Theory and Calculations

The geometries of the three lowest-energy conformers of HMHP were optimized at the hybrid density-functional theory, B3LYP,[45−47] quadratic configuration interaction including singles and doubles, QCISD,[48] and coupled cluster singles and double with perturbative triples, CCSD(T),[49−51] levels of theory with a selectively augmented cc-pVTZ (correlation consistent polarized triple-ζ)[52−54] basis set. The CCSD(T) theory is known to provide accurate molecular geometries and spectroscopic constants[55] but is computationally demanding. To reduce the computational cost, we use the aug-cc-pVTZ basis set for the two hydroxyl groups, while modeling the rest of the molecule with the cc-pVTZ basis set. This form of selective augmentation (labeled aug′-cc-pVTZ) has been shown to accurately model OH-stretching vibrations in ethylene glycol.[42] Harmonic normal-mode frequencies were calculated at the QCISD/aug′-cc-pVTZ level for the three stable conformers of HMHP. All ab initio

energy calculations were run using the computational suite MOLPRO 2002.6[56] at the University of Otago.

Vibrational OH-Stretching Model. The oscillator strength, *f*, of a transition from the ground vibrational state $|0\rangle$ to a vibrationally excited state $|\nu\rangle$ is given by[39,57]

$$f_{\nu 0} = (4.702 \times 10^{-7}\ \text{cm D}^{-2})\tilde{\nu}_{\nu 0}|\vec{\mu}_{\nu 0}|^2 \quad (1)$$

where $\tilde{\nu}_{\nu 0}$ is the wavenumber of the transition and $\vec{\mu}_{\nu 0} = \langle \nu|\vec{\mu}|0\rangle$ is the transition dipole moment matrix element in debye (D).

We have used a simple anharmonic oscillator local-mode model to characterize the OH-stretching modes. The Hamiltonian for an isolated OH-stretching oscillator can be written as a Morse oscillator:[58]

$$(H - E_{|0\rangle})/hc = \nu\tilde{\omega} - (\nu^2 + \nu)\tilde{\omega}x \quad (2)$$

where $E_{|0\rangle}$ is the energy of the vibrational ground state and $\tilde{\omega}$ and $\tilde{\omega}x$ are the local-mode frequency and anharmonicity, respectively.

The OH-stretching frequency and anharmonicity are obtained from the second (f_{ii}), third (f_{iii}), and fourth (f_{iv}) order derivatives of the potential energy with respect to the OH-stretching coordinate according to[42,59,60]

$$\tilde{\omega} = \frac{\sqrt{f_{ii}G_{ii}}}{2\pi c} \quad (3)$$

$$\tilde{\omega}x = \frac{\hbar G_{ii}}{32\pi c f_{ii}}\left(\frac{5f_{iii}^{\ 2}}{3f_{ii}} - f_{iv}\right) \quad (4)$$

where G_{ii} is the reciprocal of the OH reduced mass.

The dipole moment function is approximated by a series expansion in the internal displacement coordinate *q* about the equilibrium geometry:[58]

$$\vec{\mu}(q) = \sum_i \vec{\mu}_i q^i \quad (5)$$

where the coefficients $\vec{\mu}$ are given by

$$\vec{\mu}_i = \frac{1}{i!}\frac{\partial^i \vec{\mu}}{\partial q^i}\bigg|_e \quad (6)$$

The coefficients $\vec{\mu}_i$ are determined from an ab initio calculated one-dimensional grid of the dipole moment $\vec{\mu}(q)$.

One-dimensional grids were calculated using QCISD/aug′cc-pVTZ and CCSD(T)/aug′-cc-pVTZ at their respective optimized geometries by displacing each OH bond from equilibrium by $-0.30 < q < 0.40$ Å in steps of 0.05 Å for a total of 15 points. The required force constants are found by fitting a 12th order polynomial to the 13 points symmetrically distributed about the equilibrium bond length.[61] The dipole-moment expansion coefficients are found from a sixth order polynomial fitted to all 15 grid points.[62] The dipole moment at each grid point was determined analytically for the QCISD level of theory and numerically using a finite field of ±0.005 au for the CCSD(T) level of theory. This field size was chosen to ensure numerical stability of the higher-order dipole derivatives without perturbing the molecular system significantly.[63]

$HOCH_2O-OH$ Bond Dissociation Energy. Ab initio geometry optimizations and energy calculations of HMHP and the two photodissociation fragments, OH and OCH_2OH, at the UCCSD(T)/aug′-cc-pVTZ level were carried out to obtain an estimate of the bond dissociation energy, D_0. Zero-point vibrational energy (ZPVE) corrections were calculated with the UQCISD/aug′-cc-pVTZ method.

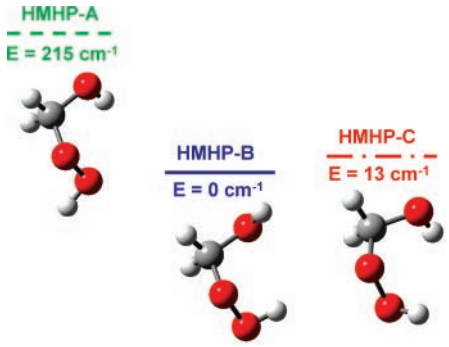

Figure 1. Energy level diagram of the relative energies of the three most stable structural conformers of hydroxymethyl hydroperoxide (HMHP), as calculated at the CCSD(T)/aug′-cc-pVTZ level including QCISD/aug′-cc-pVTZ ZPE.

D_0 was also estimated using a statistical state counting calculation using the HMHP density of states calculated by the MultiWell DenSum program.[64,65] The DenSum program calculates exact counts of sums and densities of states using the ab initio calculated normal-mode frequencies (QCISD/aug′cc-pVTZ) calculated for HMHP-B. We assume that all HMHP population excited above the dissociation threshold dissociates. Further details of the assumptions and uncertainties in this D_0 estimation follow in the Results and Discussion section on quantum yield and dissociation energy. A value for D_0 was found that gives quantum yields for the two major bands in the $4\nu_{OH}$ spectrum that match those determined by comparison of observed relative band intensities and calculated band strengths in the $4\nu_{OH}$ and $5\nu_{OH}$ regions. This estimated D_0 was subsequently used to predict atmospheric pressure quantum yields and to estimate the atmospheric vibrational overtone photolysis rate for HMHP.

Results and Discussion

Previously, the lowest-energy conformers of HMHP had been studied with the B3LYP/6-311++G(2d,2p) method.[66] We further optimized the three lowest-energy conformers to the CCSD(T)/aug′-cc-pVTZ level. The optimized structures and relative energies are shown in Figure 1 and we refer to them as HMHP-A, HMHP-B, and HMHP-C. The complete optimized geometries for these three conformers of HMHP are reported in the Supporting Information (Tables 1S−3S). In the lowest-energy conformer, HMHP-B, it is the OO−H group which donates the H atom to form a hydrogen bond. In the two higher-energy conformers, HMHP-A and HMHP-C, it is the RO−H group that donates the H atom to form a hydrogen bond. With the CCSD(T)/aug′-cc-pVTZ method, HMHP-C and HMHP-A are found to be 76 and 301 cm^{-1} higher in energy than HMHP-B. Including zero-point vibrational energy correction at the QCISD/aug′-cc-pVTZ level the energy difference becomes 13 and 215 cm^{-1}, respectively, which, assuming a Boltzmann distribution, would give approximately 44% HMHP-B, 41% HMHP-C, and 15% HMHP-A at 300 K.

OH-Stretching Spectra. The fundamental (ν_{OH}) and first overtone ($2\nu_{OH}$) OH-stretching regions of the FTIR spectrum are shown in Figures 2 and 3. The signal-to-noise ratio was not sufficient to detect any bands in the $3\nu_{OH}$ region. The entire FTIR spectrum in the range 1000−7500 cm^{-1}, this FTIR spectral information as x, y text files, a table of FTIR band positions, relative intensities and assignments, and the QCISD/aug′-cc-pVTZ calculated normal modes and intensities for the

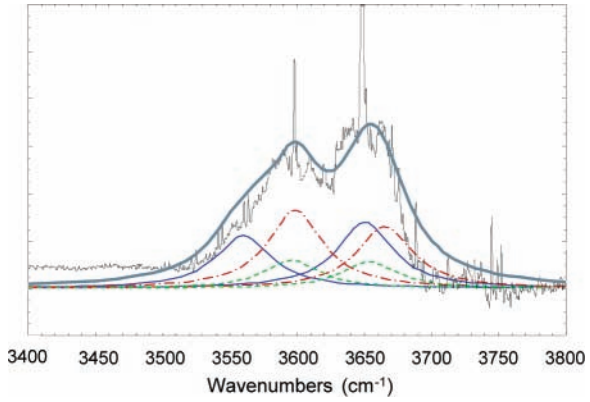

Figure 2. Experimental FTIR and simulated spectra in the fundamental ν_{OH} region of HMHP. The experimental spectrum is in black; the simulated spectra are HMHP-A (green, dashed line), HMHP-B (blue, solid line), HMHP-C (red, dash−dotted line), and the weighted sum (heavy gray line).

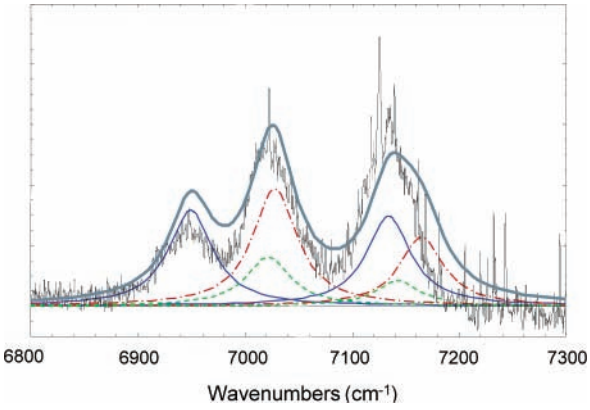

Figure 3. Experimental FTIR and simulated spectra in the first overtone $2\nu_{OH}$ region of HMHP. The experimental spectrum is in black; the simulated spectra are HMHP-A (green, dashed line), HMHP-B (blue, solid line), HMHP-C (red, dash−dotted line), and the weighted sum (heavy gray line).

three conformers are given in the Supporting Information (Figures 1S and 2S, Tables 4S and 5S, and text files). Impurities visible in the FTIR spectrum are H_2O_2, H_2O, and CO_2. The action spectra of HMHP in the $4\nu_{OH}$ and of HMHP-d_2 in the $5\nu_{OH}$ overtone regions are shown in Figures 4 and 5. The observed OH-stretching transitions and measured relative intensities are given in Table 1.

The spectra are made complex by the existence of two distinct OH chromophores and three HMHP conformers. To assign the spectra, we calculated the OH-stretching transitions of the different chromophores in the three lowest-energy structures with the anharmonic oscillator local-mode model. The CCSD-(T) calculated local-mode parameters of the different OH oscillators are given in Table 2. The calculated band positions and oscillator strengths of the OH-stretching local-mode transitions are shown in Table 3. The results obtained with the QCISD method are similar to those obtained with CCSD(T) and are not shown. The CCSD(T) frequencies are closer to the experimental band positions than those obtained with the QCISD method, alleviating the usual need for empirical scaling of local-mode parameters.[41,42]

In the $1\nu_{OH}$ region ($\sim$3600 cm^{-1}), we assign two bands, well defined by their Q-branches, to the OO−H and RO−H transitions of all conformers. This assignment is based on our calculations and is consistent with the generally lower-vibration frequency of a peroxide OH stretch versus an alcohol OH

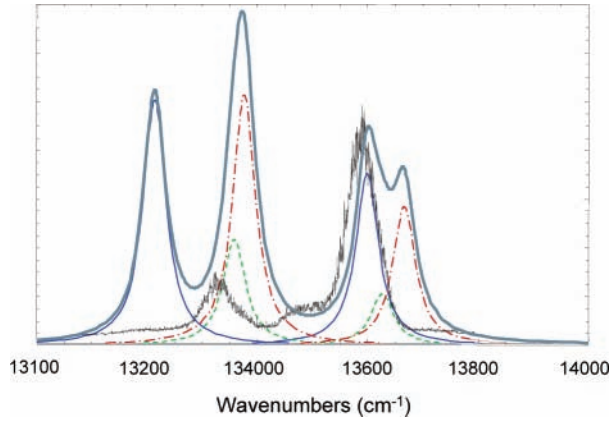

Figure 4. Experimental action and simulated(absorption) spectra in the $4\nu_{OH}$ region of HMHP. The experimental spectrum was collected monitoring $N = 1$ of the product OH (peak of product state distribution). Note that no quantum yield adjustments were made to the simulated spectra. See text for discussion. The experimental spectrum is in black; the simulated spectra are HMHP-A (green, dashed line), HMHP-B (blue, solid line), HMHP-C (red, dash−dotted line), and the weighted sum (heavy gray line).

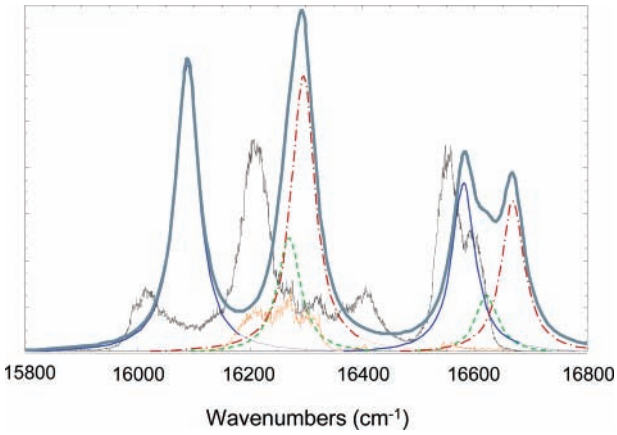

Figure 5. Experimental action and simulated spectra in the $5\nu_{OH}$ region of HMHP-d_2. The experimental spectrum was collected monitoring $N = 3$ of the product OH (peak of product state distribution). The experimental spectrum is in black; the simulated spectra are HMHP-A (green, dashed line), HMHP-B (blue, solid line), HMHP-C (red, dash−dotted line), and the weighted sum (heavy gray line).

TABLE 1: Observed OH Band Centers (in cm^{-1}), Relative Peak Intensities, and Assignments

observed band center (cm^{-1})	relative intensity[a]	assignment
3 598.1	0.70	OO−H, all three conformers
3 647.8	1.00	RO−H, all three conformers
6 947.1	0.40	OO−H, HMHP-B
7 022.9	0.85	OO−H, HMHP-A/C
7 125.4	1.00	RO−H, all three conformers
13 200	0.05	OO−H, HMHP-B
13 330	0.30	OO−H, HMHP-A/C
13 480	0.15	unassigned
13 550	1.00	RO−H, all three conformers
16 010	0.30	OO−H, HMHP-B
16 220	1.00	OO−H, HMHP-A/C
16 400	0.30	unassigned
16 550	0.95	RO−H, HMHP-A/B
16 600	0.60	RO−H, HMHP-C

[a] Measured relative intensities refer to comparison within each spectral region.

stretch,[67] and consistent with the Niki et al. assignment.[68] On the basis of the calculated band center of the RO−H transitions given in Table 3, we would not expect the transitions from the

TABLE 2: Calculated OH-Stretching Local-Mode Parameters (in cm^{-1}) Compared with Experimentally Derived Values

mode	$\tilde{\omega}$	$\tilde{\omega}x$
OOH (HMHP-A)[a]	3769.8	85.70
ROH (HMHP-A)[a]	3820.6	82.40
OOH (HMHP-B)[a]	3733.8	85.69
ROH (HMHP-B)[a]	3820.1	83.72
OOH (HMHP-C)[a]	3771.1	85.04
ROH (HMHP-C)[a]	3833.6	83.01
Experimental		
OOH (HMHP-A/C)[b]	3779	89.2
OOH (HMHP-B)[b]	3748	90.5

[a] Calculated with the CCSD(T)/aug′-cc-pVTZ method. [b] Experimental values from Birge−Spooner fit of the $2\nu_{OH}$, $4\nu_{OH}$, and $5\nu_{OH}$ bands.

TABLE 3: Calculated OH-Stretching Frequencies (in cm^{-1}) and Intensities[a]

		HMHP -A		HMHP-B		HMHP-C	
v		$\tilde{\nu}$	f	$\tilde{\nu}$	f	$\tilde{\nu}$	f
1	OOH	3 598	5.8×10^{-6}	3 562	3.9×10^{-6}	3 601	6.1×10^{-6}
	ROH	3 666	5.6×10^{-6}	3 653	4.8×10^{-6}	3 668	4.8×10^{-6}
2	OOH	7 026	8.5×10^{-7}	6 953	5.9×10^{-7}	7 032	7.7×10^{-7}
	ROH	7 147	4.3×10^{-7}	7 138	5.5×10^{-7}	7 169	4.5×10^{-7}
3	OOH	1 028	3.1×10^{-8}	10 173	2.4×10^{-8}	10 293	2.7×10^{-8}
	ROH	10 473	1.5×10^{-8}	10 456	2.0×10^{-8}	10 505	1.6×10^{-8}
4	OOH	13 365	1.6×10^{-9}	13 221	1.4×10^{-9}	13 384	1.4×10^{-9}
	ROH	13 634	7.9×10^{-10}	13 606	9.3×10^{-10}	13 674	8.0×10^{-10}
5	OOH	16 278	1.4×10^{-10}	16 098	1.3×10^{-10}	16 304	1.3×10^{-10}
	ROH	16 631	7.1×10^{-11}	16 589	7.1×10^{-11}	16 678	7.0×10^{-11}

[a] Calculated with the local-mode parameters in Table 2 and CCSD(T)/aug′-cc-pVTZ dipole moment functions.

various conformers to be resolved. However, the fundamental OO−H stretch of HMHP-B is calculated to be ∼40 cm^{-1} lower that those of HMHP-A/C and is perhaps evident as the weak shoulder to the red of the main band.

In the $2\nu_{OH}$ region (∼7000 cm^{-1}), the OO−H stretch transition of HMHP-B appears as a well resolved peak at 6947 cm^{-1}, in excellent agreement with our calculated band center of 6953 cm^{-1}. The OO−H stretch of HMHP-A/C is observed at 7023 cm^{-1}, within 7 cm^{-1} of the calculated transitions. The strongest band at 7126 cm^{-1} is assigned to the RO−H transitions of all conformers, which we calculate to lie in the range from 7138 to 7169 cm^{-1}, possibly indicating that the local-mode frequency of HMHP-C is a bit high.

The action spectrum in the $4\nu_{OH}$ region (∼13500 cm^{-1}) is shown in Figure 4. A spectrum of the contaminant species H_2O_2 was collected for this region; however, it was possible to minimize its contribution to negligible in this $4\nu_{OH}$ spectrum, and the H_2O_2 spectrum is therefore not shown. Assignment is complicated because the dissociation energy of HMHP lies in this region. At excitation energies below the dissociation threshold, D_0, the quantum yield will be nonuniform, since only vibrational states with sufficient internal energy will dissociate upon excitation by the pump laser. This suppresses the lower-energy bands relative to the higher-energy bands, producing a difference between the action spectrum and the absorption spectrum. The dominant band at 15 350 cm^{-1} is assigned to the RO−H transitions of all conformers. We assign the weaker band, around 13 330 cm^{-1}, to the OO−H transition of HMHP-A/C, with its intensity reduced by the smaller quantum yield. We do not clearly observe the OO−H transition of HMHP-B; it is further to the red, and its intensity is significantly reduced by low quantum yield.

In Figure 5 we show the action spectrum of HMHP-d_2 in the $5\nu_{OH}$ region (∼16400 cm^{-1}). This band lies significantly above the dissociation energy, so unity quantum yield is expected. We compare the HMHP-d_2 spectrum (rather than that of HMHP) with the local-mode model, because of the existence of a Fermi resonance between OH- and CH-stretch states. This resonance splits the RO−H-stretching transition in the HMHP $5\nu_{OH}$ spectrum into two bands as shown in Figure 6. The spectrum of the contaminant species H_2O_2 is shown for reference in Figure 5, since it was not possible to completely remove its contribution. The peaks at 16 550 and 16 600 cm^{-1} are assigned as the RO−H-stretch transitions of HMHP-B and HMHP-A/C, respectively. The separation of these transitions was not observed at the $4\nu_{OH}$ overtone. We assign the other strong transition at 16 220 cm^{-1} to the OO−H stretch of HMHP-A/C, with the weaker band to the red at 16 010 cm^{-1} assigned to the OO−H-stretch transition in HMHP-B.

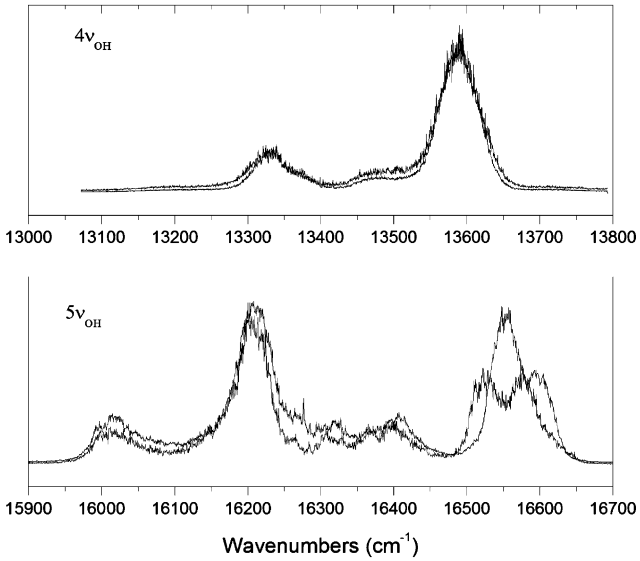

Figure 6. Action spectra of HMHP (grey) and HMHP-d_2 (black) in the $4\nu_{OH}$ and $5\nu_{OH}$ regions.

The calculated local-mode parameters of the different OH-stretching oscillators are compared to experimentally derived parameters in Table 2. The agreement is reasonable with $\tilde{\omega}_{OO-H}$ within 10 cm^{-1} and $\tilde{\omega}x_{OO-H}$ within 4 cm^{-1} of the calculated values for the OO−H mode in HMHP-A/C. We could not resolve the peaks from the RO−H for HMHP-A/C in more than one overtone and hence no local-mode parameters are derived. The reasonable agreement between these observed and unscaled calculated local-mode parameters support our assignment of the peaks.

We have simulated the HMHP absorption spectra in the $1-5\nu_{OH}$ regions. The simulated spectra are obtained by convolving each of our calculated OH-stretching transitions, given in Table 3, with a Lorentzian line shape of full-width at half-maximum 50 cm^{-1}. The predicted spectra for the three HMHP conformers are scaled by their relative Boltzmann populations. The simulated absorption bands are shown overlapped with the experimental spectra in Figures 2−5.

The simulated spectra reproduce both the positions and intensities of the major features in the $1\nu_{OH}$ and $2\nu_{OH}$ regions. The agreement in the $4\nu_{OH}$ and $5\nu_{OH}$ regions is less good because small errors in the calculated local-mode parameters are amplified[42] and because in the $4\nu_{OH}$ region the nonuniform dissociation quantum yield in the experimental spectrum is not accounted for in the simulation (discussed in the next section). In the $4\nu_{OH}$ and $5\nu_{OH}$ regions, the calculated peaks are consistently at slightly higher wavenumbers than the observed

peaks. In the $5\nu_{OH}$ region, the calculated relative intensity of the OO−H and RO−H peaks of HMHP-A/C is in good agreement with that of the experimental HMHP-d_2 spectrum. For HMHP-B, however, the intensity of the OO−H peak is overestimated relative to the RO−H peak. Disagreement in spectra can be due to errors in the calculated relative intensities of transitions of the three conformers, errors in the relative energies of the three conformers, or errors in relating action to absorption spectra. A temperature dependence study of the HMHP spectra would help constrain the relative abundance of the conformers.

The difference in the $5\nu_{OH}$ region of HMHP and HMHP-d_2 spectra (Figure 6) suggests significant coupling between the RO−H- and CH-stretching modes in the HMHP molecule. The dominant peak at 16 550 cm^{-1} in the HMHP-d_2 spectrum splits into two strong peaks in the HMHP spectrum. The smaller peak at 16 600 cm^{-1} in the HMHP-d_2 is seen as a broad shoulder in the HMHP spectrum. The CH-stretching fundamental is observed in the FTIR spectrum around 2940 cm^{-1}. The combination band $4\nu_{OH} + 1\nu_{CH}$ is therefore ($4\nu_{OH} + 1\nu_{CH} = 16\,540$ cm^{-1}) near resonant with the $5\nu_{OH}$ band ($5\nu_{OH} = 16\,550$ cm^{-1}), and significant mixing of states occurs. A similar coupling has been observed in formic acid[69] and in methanol.[70] In both of these cases, the coupled CH modes are trans in configuration to the OH bond. In HMHP, the CH bonds are out of the H−O−C plane, with dihedral angles of 122° for one of the CH stretches, and 55°, 168°, and 43° for the other CH stretch in HMHP-A, -B, and -C, respectively. Only the most stable HMHP-B conformer has a nearly trans configuration of the resonant OH and CH modes. This is the conformer for which we see resonance coupling, consistent with previous studies of coupling across bonds.

The unassigned weak bands around 13 480 and 16 400 cm^{-1} in the $4\nu_{OH}$ and $5\nu_{OH}$ overtones may reflect additional conformers of HMHP or combination bands which borrow intensity from the OH-stretch bright states, for example with HOOC torsional modes. There is some additional discrepancy in the spectra around 16200−16300 cm^{-1}, indicating more H_2O_2 contaminant in the HMHP-d_2 sample than in the HMHP.

Quantum Yield and Dissociation Energy. Comparison of our observed spectrum in the $4\nu_{OH}$ region with the other OH regions, particularly the suppression of the OO−H band, indicates that D_0 is larger than 13 300 cm^{-1}. Our UCCSD(T)/aug′-cc-pVTZ calculated dissociation energy D_0, including UQCISD/aug′-cc-pVTZ ZPVE correction, is 14 484 cm^{-1} (173.2 kJ/mol). This calculated D_0 value is above the location of the $4\nu_{OH}$ spectrum and would result in very low dissociation quantum yield for all transitions in the $4\nu_{OH}$ region. Previously, D_0 has been calculated to be 13 600 cm^{-1} (162.7 kJ/mol) and 15 320 cm^{-1} (183.3 kJ/mol) with the CCSD(T)/6-311+G(2d,-2p) and CBS-QB3/6-311G(2d,d,p) methods, respectively.[66,71] Both of these calculations included single point energies at the B3LYP/6-31G(d,p) geometry. To date, no experimental D_0 has been determined.

We estimate the quantum yield of the bands in the $4\nu_{OH}$ region by comparing the observed and calculated intensities in the $4\nu_{OH}$ and $5\nu_{OH}$ regions. The band intensities are corrected for the difference in pump laser power and for differences in the measured percentage of the total population contained in the probed OH quantum state (~40% in $N = 1$ for $4\nu_{OH}$ and ~20% in $N = 3$ for $5\nu_{OH}$). We apply a further correction to account for the differences in the rate of appearance of OH following the pump laser. Although we observe essentially instantaneous production (<5 ns) of OH from excitation throughout the $5\nu_{OH}$ region, OH appears with a time constant that varies from 30 to 50 ns in the $4\nu_{OH}$ region.[72] Because the spectrum shown in Figure 4 was obtained before the complete evolution of the photodissociation in $4\nu_{OH}$, we correct these band intensities by extrapolation to long probe delay time (correction of order 40−50%).

The derived ratio of the peak intensity of the RO−H band in $4\nu_{OH}$ to that of $5\nu_{OH}$ region is 2 ± 0.5, where the uncertainty arises primarily from the intensity scaling issues discussed above. The ratio of the intensities calculated from the local-mode model for these transitions is ~12. Thus, we estimate that the quantum yield at 13 550 cm^{-1} is 0.17 ± 0.05.

The analogous ratio of the integrated intensity of the OO−H band for HMHP-A/C (corrected as discussed above) in the $4\nu_{OH}$ to $5\nu_{OH}$ region is 0.6 ± 0.3. The calculated intensity ratio of these transitions is about 11; hence, the quantum yield at 13 330 cm^{-1} is 0.05 ± 0.03. The OO−H transition of HMHP-B is clearly observed in the $5\nu_{OH}$ region but is very weak in the $4\nu_{OH}$ region.

Simple state counting can be used to estimate a dissociation energy (D_0) that is consistent with the observed quantum yields. At 80 mTorr pressure and 80 ns pump−probe delay, the photodissociation occurs in an essentially collision-free environment. Under these conditions, the quantum yield is a measure of the fraction of HMHP vibrational states with energy above D_0 immediately after laser excitation. We estimate D_0 by shifting a thermalized (298 K) HMHP internal energy distribution upward by the photon energies 13 330 and 13 550 cm^{-1} and determining the value of D_0 required to give the observed quantum yields: $\Phi(13\,550\ cm^{-1}) = 0.17 \pm 0.05$ and $\Phi(13\,330\ cm^{-1}) = 0.05 \pm 0.03$. We use the vibrational frequencies calculated at QCISD/aug′-cc-pVTZ for HMHP−B (Table 5S) to determine the density of states for the initial thermalized HMHP sample, using the MultiWell program DenSum.[65] Each of these states is then shifted upward by the same photon energy to obtain the vibrationally excited-state distribution in which the observed fraction of above-threshold states (Φ) corresponds to a specific D_0. This calculation assumes that there is no barrier to dissociation and that the energy distribution in the excited state is statistical. Most dissociation processes into radical fragments are barrierless because of the high efficiency of the recombination process, so there is not likely to be a barrier on the electronic surface of dissociation to $OH + HOCH_2O$.

Within the context of this model, a value of D_0 between 13 950 and 14 150 cm^{-1} (166.9−169.3 kJ/mol) is consistent with the estimated quantum yields; however, considerations such as uncertainties in the calculated room-temperature density of states and relative abundances of conformers, the possible presence of state mixing or hot bands, and the possibility of a barrier to dissociation or nonstatistical dissociation are not included. Therefore, our confidence in the estimate of D_0 is lower. Temperature-dependent measurements or combined absorption and action spectroscopy measurements would help to reduce this uncertainty. A forthcoming phase-space theory analysis of the OH fragment rotational-state distribution will provide a complementary estimate of D_0 and an additional constraint on its value.[72]

Atmospheric Importance of Overtone Photodissociation. We estimate the clear-sky photolysis rate for HMHP arising from the $4\nu_{OH}$ and $5\nu_{OH}$ transitions from

$$J(\mathrm{HMHP}) = \int \Phi(\nu)\,\sigma(\nu)\,I(\nu)\,\mathrm{d}\nu \cong \langle I(\nu)\rangle \int \Phi(\nu)\,\sigma(\nu)\,\mathrm{d}\nu \quad (7)$$

where $\Phi(\nu)$ is the estimated quantum yield of photodissociation

TABLE 4: Calculated Integrated Absorption Cross Sections, Dissociation Quantum Yields, Solar Spectral Actinic Flux, and Resulting Clear-Sky Atmospheric Photodissociation Rates for Overtone Bands of HMHP

	band center (cm^{-1})	integrated cross section[a] (cm^2 molecule^{-1} cm^{-1})	quantum yield	solar flux[b] (photons cm^{-2} s^{-1} cm^{-1})	photolysis rate (s^{-1})
$4\nu_{OO-H}$	13 330	1.27×10^{-21}	~0.0002	2.67×10^{13}	$\sim 6.8 \times 10^{-12}$
$4\nu_{RO-H}$	13 550	7.58×10^{-22}	~0.0004	2.58×10^{13}	$\sim 7.8 \times 10^{-12}$
$5\nu_{OO-H}$	16 200	1.17×10^{-22}	1	2.05×10^{13}	2.4×10^{-9}
$5\nu_{RO-H}$	16 550	6.25×10^{-23}	1	1.91×10^{13}	1.2×10^{-9}
J(total)					3.6×10^{-9}

[a] Cross sections are weighted averages based on a population that is 44% HMHP-B, 41% HMHP-C, and 15% HMHP-A. [b] From Seinfeld & Pandis[6] Table 3.1, converted from units of W m^{-2} nm^{-1}.

for atmospheric conditions, $\int\sigma(\nu)\,d\nu$ is the integrated absorption cross-section, which is related to the calculated oscillator strength by the following relation:[73]

$$\int \sigma(\nu)\,d\nu = \frac{f}{1.1296 \times 10^{12}} \frac{\text{cm}^2}{\text{molecule cm}} \qquad (8)$$

and $I(\nu)$ is the frequency-dependent solar spectral actinic flux at the top of the atmosphere. For clear-sky conditions, the atmosphere is essentially transparent at these frequencies, so this is approximately equal to the solar flux at the ground.

The quantum yield in the $4\nu_{OH}$ band is estimated from a comparison of the atmospheric pressure collision rate with observed dissociation rates. The initial percentage of a thermal population above the threshold is only 5% for the 13 330 cm^{-1} band and 17% for the 13 550 cm^{-1} band, as determined by the quantum yields determined above. Dissociation is observed to be slow. This means that at 1 atm total pressure, collisional deactivation will dominate the rate of removal of this small above-threshold population by about 2 orders of magnitude over dissociation. The initial above-threshold population multiplied by the ratio of the dissociation rate to the collision rate is taken as the estimated quantum yield for the two bands in the $4\nu_{OH}$ region.

Results for the four $4\nu_{OH}$ and $5\nu_{OH}$ transitions are given in Table 4. The contributions from $4\nu_{OH}$ are negligible because of the very low estimated quantum yields at atmospheric pressure. The integrated cross sections shown are based on the average of the cross sections of the three conformers, weighted by their relative contributions. The total overtone mediated photolysis rate is estimated to be 3.6×10^{-9} s^{-1}. The atmospheric photolysis rate of HMHP via vibrational-overtone excitation is much slower than other loss processes for this molecule. For comparison, photolysis in the UV is estimated by Bauerle and Moortgat to be $\sim 3 \times 10^{-6}$ s^{-1} at ground level. Loss by reaction with OH or rainout and deposition are expected to be even faster.[28]

Conclusions

The OH-vibrational spectroscopy of hydroxymethyl hydroperoxide (HMHP) has been investigated experimentally and theoretically. We have assigned contributions to the observed spectra from both OH chromophores (the R−OH and O−OH ends) and from multiple stable conformers of HMHP. The effect of varying quantum yield is apparent in the $4\nu_{OH}$ action spectrum. We estimate the quantum yield as a function of excitation energy using statistical state counting and evaluate the atmospheric importance of this overtone-initiated photodissociation process. We conclude that the atmospheric lifetime of HMHP is not significantly influenced by vibrationally-mediated photodissociation.

Acknowledgment. The authors thank Mitchio Okumura, Daniel Schofield, Daryl Howard, and John Barker for valuable discussions. J.L.F. gratefully acknowledges funding provided by an American Association of University Women Dissertation Fellowship, and J.R.L. gratefully acknowledges a Top Achiever Doctoral scholarship from the Tertiary Education Commission. Funding for this work was provided by grants to P.O.W. from the National Science Foundation Division of Atmospheric Sciences (Grant ATM-0432377), to A.S. from the National Science Foundation Division of Chemistry (Grant CHE-0211496), and to H.G.K. from the Marsden Fund administered by the Royal Society of New Zealand. P.O.W. thanks the Department of Chemistry, Otago University, for support during sabbatical leave.

Supporting Information Available: Optimized geometries of three lowest-energy conformers of HMHP as calculated at CCSD(T)/aug′-cc-pVTZ (Tables 1S−3S); FTIR spectra of HMHP 1000−4000 cm^{-1} collected with an extended KBr beam splitter and 3500−7500 cm^{-1} collected with a CaF_2 beam splitter with reference H_2O_2 shown (Figures 1S & 2S); separate text files (.txt) containing the above HMHP FTIR spectra in x, y form; table of FTIR band positions, intensities, and assignments (Table 4S); normal-mode frequencies and intensities for three HMHP conformers calculated at QCISD/aug′-cc-pVTZ (Table 5S). This material is available free of charge via the Internet at http://pubs.acs.org.

References and Notes

(1) Reeves, C. E.; Penkett, S. A. *Chem. Rev.* **2003**, *103*, 5199.

(2) Lee, M. H.; Heikes, B. G.; O'Sullivan, D. W. *Atmospheric Environment* **2000**, *34*, 3475.

(3) Gunz, D. W.; Hoffmann, M. R. *Atmos. Environ.* **1990**, *24*, 1601.

(4) Lind, J. A.; Lazrus, A. L.; Kok, G. L. *J. Geophys. Res., (Atmos.)* **1987**, *92*, 4171.

(5) Zhou, X. L.; Lee, Y. N. *J. Phys. Chem.* **1992**, *96*, 265.

(6) Seinfeld, J. H.; Pandis, S. N. *Atmospheric Chemistry and Physics*; John Wiley & Sons: New York, 1998.

(7) Becker, K. H.; Brockmann, K. J.; Bechara, J. *Nature* **1990**, *346*, 256.

(8) Gab, S.; Hellpointner, E.; Turner, W. V.; Korte, F. *Nature* **1985**, *316*, 535.

(9) Horie, O.; Neeb, P.; Limbach, S.; Moortgat, G. K. *Geophys. Res. Lett.* **1994**, *21*, 1523.

(10) Neeb, P.; Sauer, F.; Horie, O.; Moortgat, G. K. *Atmos. Environ.* **1997**, *31*, 1417.

(11) Sauer, F.; Schafer, C.; Neeb, P.; Horie, O.; Moortgat, G. K. *Atmos. Environ.* **1999**, *33*, 229.

(12) Hasson, A. S.; Orzechowska, G.; Paulson, S. E. *J. Geophys. Res., (Atmos.)* **2001**, *106*, 34131.

(13) Grossmann, D.; Moortgat, G. K.; Kibler, M.; Schlomski, S.; Bachmann, K.; Alicke, B.; Geyer, A.; Platt, U.; Hammer, M. U.; Vogel, B.; Mihelcic, D.; Hofzumahaus, A.; Holland, F.; Volz-Thomas, A. *J. Geophys. Res., (Atmos.)* **2003**, *108*.

(14) Francois, S.; Sowka, I.; Monod, A.; Temime-Roussel, B.; Laugier, J. M.; Wortham, H. *Atmos. Res.* **2005**, *74*, 525.

(15) Moortgat, G. K.; Grossmann, D.; Boddenberg, A.; Dallmann, G.; Ligon, A. P.; Turner, W. V.; Gab, S.; Slemr, F.; Wieprecht, W.; Acker, K.; Kibler, M.; Schlomski, S.; Bachmann, K. *J. Atmos. Chem.* **2002**, *42*, 443.
(16) Weinstein-Lloyd, J. B.; Lee, J. H.; Daum, P. H.; Kleinman, L. I.; Nunnermacker, L. J.; Springston, S. R. *J. Geophys. Res., (Atmos.)* **1998**, *103*, 22361.
(17) Staffelbach, T.; Neftel, A.; Blatter, A.; Gut, A.; Fahrni, M.; Stahelin, J.; Prevot, A.; Hering, A.; Lehning, M.; Neininger, B.; Baumle, M.; Kok, G. L.; Dommen, J.; Hutterli, M.; Anklin, M. *J. Geophys. Res., (Atmos.)* **1997**, *102*, 23345.
(18) Lee, J. H.; Leahy, D. F.; Tang, I. N.; Newman, L. *J. Geophys. Res., (Atmos.)* **1993**, *98*, 2911.
(19) Lee, M.; Heikes, B. G.; Jacob, D. J.; Sachse, G.; Anderson, B. *J. Geophys. Res., (Atmos.)* **1997**, *102*, 1301.
(20) Sauer, F.; Schuster, G.; Schafer, C.; Moortgat, G. K. *Geophys. Res. Lett.* **1996**, *23*, 2605.
(21) Sauer, F.; Limbach, S.; Moortgat, G. K. *Atmos. Environ.* **1997**, *31*, 1173.
(22) Jackson, A. V.; Hewitt, C. N. *Atmos. Environ.* **1996**, *30*, 819.
(23) Kok, G. L.; McLaren, S. E.; Staffelbach, T. A. *J. Atmos. Ocean. Technol.* **1995**, *12*, 282.
(24) Tremmel, H. G.; Junkermann, W.; Slemr, F. *J. Geophys. Res., (Atmos.)* **1993**, *98*, 1083.
(25) Fels, M.; Junkermann, W. *Geophys. Res. Lett.* **1994**, *21*, 341.
(26) Hellpointner, E.; Gab, S. *Nature* **1989**, *337*, 631.
(27) Hewitt, C. N.; Kok, G. L. *J. Atmos. Chem.* **1991**, *12*, 181.
(28) Bauerle, S.; Moortgat, G. K. *Chem. Phys. Lett.* **1999**, *309*, 43.
(29) O'Sullivan, D. W.; Lee, M. Y.; Noone, B. C.; Heikes, B. G. *J. Phys. Chem.* **1996**, *100*, 3241.
(30) Su, F.; Calvert, J. G.; Shaw, J. H.; Niki, H.; Maker, P. D.; Savage, C. M.; Breitenbach, L. D. *Chem. Phys. Lett.* **1979**, *65*, 221.
(31) Roehl, C. M.; Nizkorodov, S. A.; Zhang, H.; Blake, G. A.; Wennberg, P. O. *J. Phys. Chem. A* **2002**, *106*, 3766.
(32) Matthews, J.; Sharma, R.; Sinha, A. *J. Phys. Chem. A* **2004**, *108*, 8134.
(33) Fry, J. L.; Nizkorodov, S. A.; Okumura, M.; Roehl, C. M.; Francisco, J. S.; Wennberg, P. O. *J. Chem. Phys.* **2004**, *121*, 1432.
(34) Matthews, J.; Sinha, A. *J. Chem. Phys.* **2005**, *122*.
(35) Roehl, C. M.; Fry, J. L.; Marka, Z.; Wennberg, P. O., *to be submitted for publication*, 2006.
(36) Henry, B. R. *Acc. Chem. Res.* **1987**, *20*, 429.
(37) Henry, B. R. *Acc. Chem. Res.* **1977**, *10*, 207.
(38) Child, M. S.; Halonen, L. *Adv. Chem. Phys.* **1984**, *57*, 1.
(39) Kjaergaard, H. G.; Yu, H. T.; Schattka, B. J.; Henry, B. R.; Tarr, A. W. *J. Chem. Phys.* **1990**, *93*, 6239.
(40) Kjaergaard, H. G.; Low, G. R.; Robinson, T. W.; Howard, D. L. *J. Phys. Chem. A* **2002**, *106*, 8955.
(41) Low, G. R.; Kjaergaard, H. G. *J. Chem. Phys.* **1999**, *110*, 9104.
(42) Howard, D. L.; Jørgensen, P.; Kjaergaard, H. G. *J. Am. Chem. Soc.* **2005**, *127*, 17096.
(43) Marklund, S. *Acta Chem. Scand.* **1971**, *25*, 3517.
(44) Dutton, G.; Barnes, R. J.; Sinha, A. *J. Chem. Phys.* **1999**, *111*, 4976.
(45) Becke, A. D. *Phys. Rev. A: At., Mol.,Opt. Phys.* **1988**, *38*, 3098.
(46) Becke, A. D. *J. Chem. Phys.* **1993**, *98*, 1372.
(47) Lee, C. T.; Yang, W. T.; Parr, R. G. *Phys. Rev. B: Condens. Matter* **1988**, *37*, 785.
(48) Pople, J. A.; Headgordon, M.; Raghavachari, K. *J. Chem. Phys.* **1987**, *87*, 5968.
(49) Purvis, G. D.; Bartlett, R. J. *J. Chem. Phys.* **1982**, *76*, 1910.
(50) Raghavachari, K.; Trucks, G. W.; Pople, J. A.; Headgordon, M. *Chem. Phys. Lett.* **1989**, *157*, 479.
(51) Watts, J. D.; Gauss, J.; Bartlett, R. J. *J. Chem. Phys.* **1993**, *98*, 8718.
(52) Dunning, T. H. *J. Chem. Phys.* **1989**, *90*, 1007.
(53) Kendall, R. A.; Dunning, T. H.; Harrison, R. J. *J. Chem. Phys.* **1992**, *96*, 6796.
(54) Woon, D. E.; Dunning, T. H. *J. Chem. Phys.* **1993**, *98*, 1358.
(55) Helgaker, T.; Ruden, T. A.; Jorgensen, P.; Olsen, J.; Klopper, W. *J. Phys. Org. Chem.* **2004**, *17*, 913.
(56) Amos, R. D.; Bernhardsoon, A.; Berning, A.; Celani, P.; Cooper, D. L.; Deegan, M. J. O.; Dabbyn, A. J.; Eckert, F.; Hampel, C.; Hetzer, G.; Knowles, P. J.; Korona, T.; Lindh, R.; Lloyd, A. W.; McNicholas, S. J.; Manby, F. R.; Meyer, W.; Mura, M. E.; Nicklass, A.; Palmieri, P.; Pitzer, R.; Rauhut, G.; Schütz, M.; Schumann, U.; Stoll, H.; Stone, A. J.; Tarroni, R.; Thorsteinsson, T.; Werner, H.-J. *MOLPRO, a Package of Ab Initio Programs Designed by H.-J. Werner and P. J. Knowles*, version 2002.6; Cardiff University: Cardiff, U.K.
(57) Atkins, P. W. *Molecular Quantum Mechanics*, 2nd ed.; Oxford University Press: New York, 1983.
(58) Kjaergaard, H. G.; Turnbull, D. M.; Henry, B. R. *J. Chem.Phys.* **1993**, *99*, 9438.
(59) Herzberg, G. *Molecular Spectra and Molecular Structure I. Spectra of Diatomic Molecules*; D. Van Nostrand Company, Inc.: Princeton, NY, 1950.
(60) Kjaergaard, H. G. Unpublished work.
(61) Schofield, D. P.; Kjaergaard, H. G.; Matthews, J.; Sinha, A. *J. Chem. Phys.* **2005**, *123*.
(62) Rong, Z. M.; Kjaergaard, H. G. *J. Phys. Chem. A* **2002**, *106*, 6242.
(63) Pecul, M.; Saue, T.; Ruud, K.; Rizzo, A. *J. Chem. Phys.* **2004**, *121*, 3051.
(64) Barker, J. R. *Int. J. Chem. Kinet.* **2001**, *33*, 232.
(65) Barker, J. R. MultiWell, version 1.2.1; 2002, http://data.engin.umich.edu/multiwell.
(66) Crehuet, R.; Anglada, J. M.; Bofill, J. M. *Chem.—Eur. J.* **2001**, *7*, 2227.
(67) Herzberg, G. *Molecular Spectra and Molecular Structure Volume II: Infrared and Raman Spectra of Polyatomic Molecules*; Krieger Publishing Company: Malabar, Florida, 1945.
(68) Niki, H.; Maker, P. D.; Savage, C. M.; Breitenbach, L. P. *Chem. Phys. Lett.* **1980**, *75*, 533.
(69) Howard, D. L.; Kjaergaard, H. G. *J. Chem. Phys.* **2004**, *121*, 136.
(70) Boyarkin, O. V.; Lubich, L.; Settle, R. D. F.; Perry, D. S.; Rizzo, T. R. *J. Chem. Phys.* **1997**, *107*, 8409.
(71) Hasson, A. S.; Chung, M. Y.; Kuwata, K. T.; Converse, A. D.; Krohn, D.; Paulson, S. E. *J. Phys. Chem. A* **2003**, *107*, 6176.
(72) Matthews, J.; Fry, J. L.; Roehl, C. M.; Wennberg, P. O.; Sinha, A., submitted for publication, 2006.
(73) Bernath, P. F. *Spectra of Atoms and Molecules*, 2nd ed.; Oxford University Press: New York, 2005.